Purdue University
Purdue e-Pubs

Birck and NCN Publications | Birck Nanotechnology Center

3-1-2011

Coherent Electron Transport by Adiabatic Passage in an Imperfect Donor Chain

Rajib Rahman
Sandia National Laboratories

Richard P. Muller
Sandia National Laboratories

James E. Levy
Sandia National Laboratories

Malcolm S. Carroll
Sandia National Laboratories

Gerhard Klimeck
NCN, Purdue University, gekco@purdue.edu

See next page for additional authors

Follow this and additional works at: http://docs.lib.purdue.edu/nanopub

Part of the Nanoscience and Nanotechnology Commons

Rahman, Rajib; Muller, Richard P.; Levy, James E.; Carroll, Malcolm S.; Klimeck, Gerhard; Greentree, Andrew D.; and Hollenberg, Lloyd C. L., "Coherent Electron Transport by Adiabatic Passage in an Imperfect Donor Chain" (2011). *Birck and NCN Publications.* Paper 720.
http://docs.lib.purdue.edu/nanopub/720

This document has been made available through Purdue e-Pubs, a service of the Purdue University Libraries. Please contact epubs@purdue.edu for additional information.

Authors
Rajib Rahman, Richard P. Muller, James E. Levy, Malcolm S. Carroll, Gerhard Klimeck, Andrew D. Greentree, and Lloyd C. L. Hollenberg

This article is available at Purdue e-Pubs: http://docs.lib.purdue.edu/nanopub/720

Coherent electron transport by adiabatic passage in an imperfect donor chain

Rajib Rahman,[1,*] Richard P. Muller,[1,†] James E. Levy,[1] Malcolm S. Carroll,[1] Gerhard Klimeck,[2] Andrew D. Greentree,[3] and Lloyd C. L. Hollenberg[3]

[1]*Sandia National Laboratories, Albuquerque, New Mexico 87185, USA*

[2]*Network for Computational Nanotechnology, Purdue University, West Lafayette, Indiana 47907, USA*

[3]*Center for Quantum Computer Technology, School of Physics, University of Melbourne, Victoria 3010, Australia*

(Received 6 August 2010; revised manuscript received 22 September 2010; published 18 October 2010)

Coherent tunneling adiabatic passage (CTAP) has been proposed as a long-range physical quantum bits (qubit) transport mechanism in solid-state quantum computing architectures. Although the mechanism can be implemented in either a chain of quantum dots or donors, a one-dimensional chain of donors in Si is of particular interest due to the natural confining potential of donors that can, in principle, help reduce the gate densities in solid-state quantum computing architectures. Using detailed atomistic modeling, we investigate CTAP in a more realistic triple donor system in the presence of inevitable fabrication imperfections. In particular, we investigate how an adiabatic pathway for CTAP is affected by donor misplacements and propose schemes to correct for such errors. We also investigate the sensitivity of the adiabatic path to gate voltage fluctuations. The tight-binding based atomistic treatment of straggle used here may benefit understanding of other donor nanostructures, such as donor-based charge and spin qubits. Finally, we derive an effective 3×3 model of CTAP that accurately resembles the voltage tuned lowest energy states of the multimillion atom tight-binding simulations and provides a translation between intensive atomistic Hamiltonians and simplified effective Hamiltonians while retaining the relevant atomic-scale information. This method can help characterize multidonor experimental structures quickly and accurately even in the presence of imperfections, overcoming some of the numeric intractabilities of finding optimal eigenstates for nonideal donor placements.

DOI: 10.1103/PhysRevB.82.155315 PACS number(s): 05.60.Gg, 73.63.Kv, 73.21.La

I. INTRODUCTION

Silicon quantum bits (qubits) are pursued due to the promise of long spin coherence times and the processing expertise of the semiconductor industry that potentially could produce a quantum computer (QC). Over the past decade, many different Si qubits have been proposed. Some of these are based on nuclear[1] or electronic spins[2,3] of donors while others are based on electronic spins in lithographically or electrostatically defined quantum dots[4,5] and still others are based on the localized charge states[6] of confined electrons.

QC architectures will benefit greatly if long-range coherent quantum transport schemes can be incorporated into the architecture for efficient transfer of the qubit state to different areas of the QC. In Ref. 7, a two-dimensional (2D) bilinear array architecture for donor qubits was presented that utilized a novel nonlocal quantum transport mechanism called coherent tunneling adiabatic passage (CTAP).[8]

In essence, CTAP is a solid-state analog of the well-known stimulated raman adiabatic passage (STIRAP) protocol of quantum optics.[9] It is ideally suited to physically transporting quantum information across a chain of donors or quantum dots. STIRAP has been recently demonstrated in optical waveguides using photons.[10–12] Apart from dot[8] and donor[7] based CTAP for quantum information transport, CTAP has also been proposed for transporting single atoms[13,14] and Bose-Einstein condensates.[15,16] In previous works, comparisons have been made between the solid-state and quantum optics versions of CTAP.[17,18] Recent works have explored alternate coupling schemes[19] and CTAP based interferometry[20] in donor nanostructures. Since triple dot structures have already been fabricated,[21–25] solid-state CTAP may not be far from reality.

In a system of tunnel-coupled donors or quantum dots, CTAP can be realized by modulating barrier gates [Fig. 1(a)] adiabatically in a counter intuitive pulsing sequence.[8] The protocol begins with an electron localized at one end of the chain in a superposition of its up and down spin states, and ends with the electron transported to the other end of the chain while retaining the quantum superposition in the spin basis [Fig. 1(b)]. At all times during the transfer, there is negligible occupation probability of the electron at any point along the chain except for the ends. In effect, the protocol realizes certain pathways in the eigenspace through sensitive control of the molecular states of the donors or the dots. The method is expected to reduce gate densities relative to other quantum transport architectures in QCs, such as electron shuttling on the surface.[26]

Bottom-up approaches have been successful in placing single donors in Si with a precision of 1 nm.[27] Recently, a one-dimensional wire of donors has been fabricated by scanning tunnel microscope (STM) patterning single phosphorus donors in Si.[28] Other recent STM patterned structures include a 2D delta-doped layer of P donors for gating other nanostructures,[29] a single P donor surrounded by four leads,[30] and a quantum dot formed by patterning a few donors.[31] Top-down approaches by selective ion implantation have also been successful in fabricating few donor devices.[32] In Ref. 33, strategies to build a few donor CTAP device by ion implantation was explored. Such experimental progress in donor placement motivates the examination of donor-CTAP's robustness to nonideal placement of the donors and voltage fluctuations.

Since the interdonor tunnel coupling is sensitive to the relative locations of the donors, even small placement errors of a lattice constant or less are likely to affect the adiabatic

 ©2010 The American Physical Society

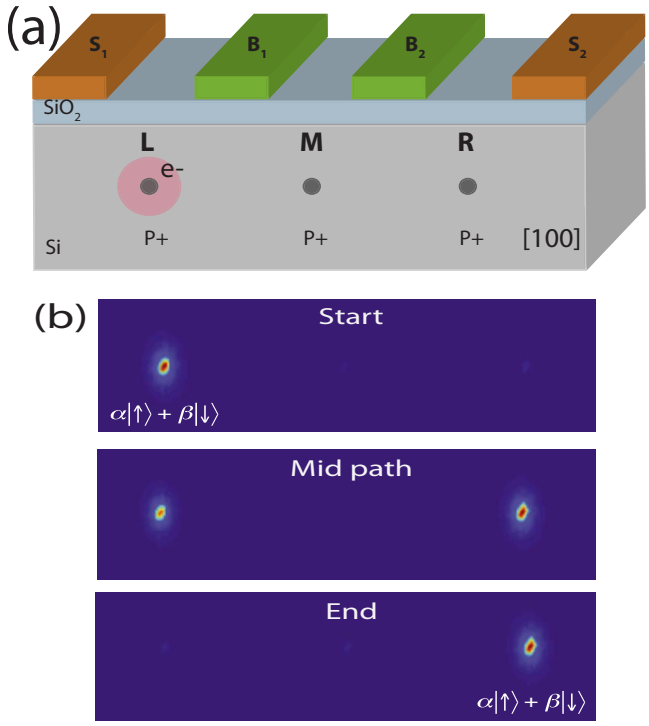

FIG. 1. (Color online) (a) A three-donor CTAP device with surface (S) gates and barrier (B) gates. The system has three ionized donors (L=Left, M=Middle, R=Right) and one bound electron. The device size is 60 nm$\times$30.4 nm$\times$30.4 nm. (b) The localization of the donor electron at three different voltage configurations in their stepped sequence. Although CTAP is a charge transport mechanism, in QC architectures it can be used to transport the spin superposition from the left to the right donor.

pathway in practical implementations of CTAP. In fact, this donor straggle problem occurs in all donor qubits, whether spin or charge based. In the Kane qubit,[1] the interdonor exchange energy has been shown to oscillate with relative donor separations.[34] In a donor charge qubit, the symmetric-antisymmetric gap (Δ_{SAS}) also exhibits oscillations as a function of donor separation and orientation.[35] The sensitivity of these parameters occur both due to the exponential falloff of the envelope wave function and due to the rapidly oscillating Bloch functions resulting from the momentum states near the conduction band valleys of the host. A resolution to this problem is to experimentally characterize each donor qubit and their interactions,[36–38] and obtain voltage pulses that correct for these straggle effects.

In a previous work,[39] the existence of an adiabatic pathway in an ideal triple donor chain was established using large scale atomistic tight-binding (TB) simulations. For the specific donor configuration in consideration, a set of voltages was found to implement a complete transfer sequence of the electron from one end of the chain to the other, thereby proving that a translation of this protocol from the quantum optics framework to a real solid-state nanostructure is valid and feasible.

In this work, we investigate the robustness of the adiabatic path against imperfections such as donor straggle and gate voltage fluctuations. We also develop a general model that provides improved insight about the tunnel couplings and on-site energies of the multimillion atom system. The model can assist experiments to characterize donor nanostructures efficiently, and can help to design voltage pulses to correct for straggle. Although we restrict our attention to a triple donor chain, the methods and the results presented here can be easily translated to other three-dimensional (3D) confined nanostructures in silicon and longer CTAP chains.

We have employed atomistic TB theory,[40] as this technique provides a highly accurate description of impurities in silicon[41–44] and allows the fast solution of million atom systems.[45] This method also treats the full band structure of the host, and provides a unified framework to treat realistic geometries, gate voltages, and disorder in an atomistic setting.[46]

This paper is organized as follows. In Sec. II, we describe the specifics of the nanostructure considered here, and introduce a solution for the adiabatic pathway with ideal donor placements.[39] Section III elaborates on the method of calculation. Section IV describes the results in detail. We show direct TB simulations of the effect of straggle and its corrections. We also show an effective 3×3 matrix model based on TB wave functions that can capture the effect of the gates and the details of the straggle.

II. ADIABATIC PATH IN AN IDEAL TRIPLE DONOR CTAP DEVICE

The CTAP device used in this work is shown in Fig. 1(a). For consistency, we have used the same device as in Ref. 39, except displacing the donor positions to study effects of straggle. The structure consists of about 3.5 million Si atoms with one electron bound across three ionized P donors. Two symmetry gates and two barrier gates, each of 10 nm width, are placed above a 5 nm thick oxide layer on top of the Si lattice. Ideally, the barrier (B) gates modulate the tunnel barriers between the donors whereas the symmetry (S) gates detune the energies of the end donors. The donors are buried 15 nm below the oxide, and are also placed 15 nm apart from each other in the [100] direction in the ideal case. The closeness of the gates in this particular device gives rise to significant crosstalk. Further details of the structure can be found in Ref. 39.

The three donor system can be conceptually understood with an effective 3×3 Hamiltonian,

$$\begin{pmatrix} 0 & t_{LM} & 0 \\ t_{LM} & 0 & t_{MR} \\ 0 & t_{MR} & 0 \end{pmatrix}, \tag{1}$$

where t_{LM} and t_{MR} are the gate voltage tuned tunnel couplings between the donors L, M, and R. We assume a simplified case for this discussion such that the donor on-site energies are aligned, which can be practically achieved via tuning by the symmetry gates S_1 and S_2. The lowest states of this Hamiltonian are,

$$|\Psi_j\rangle = \alpha_j|L\rangle + \beta_j|M\rangle + \gamma_j|R\rangle, \tag{2}$$

where α_j, β_j, and γ_j are the coefficients of the donor states $|L\rangle$, $|M\rangle$, and $|R\rangle$, respectively, for the eigenstate j. Here, j

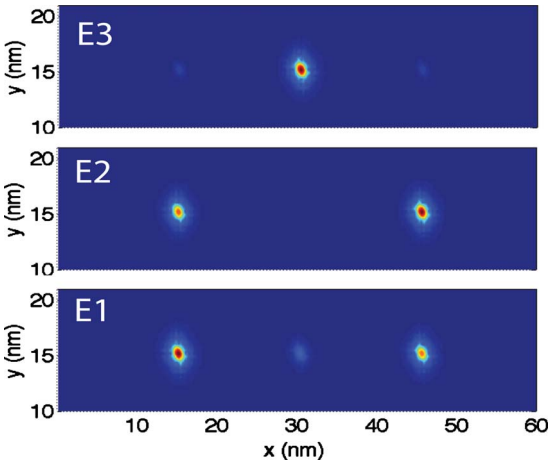

FIG. 2. (Color online) (a) The lowest three eigenstates of the system near the midpoint of an adiabatic path for CTAP. These were obtained from tight-binding simulations of the device containing about 3.5 million atoms. The transfer takes effect through the first excited state of the system (E2), in which the electron density diminishes at the center donor. This point in the adiabatic path was realized for the gate configuration $(V_{S1},V_{B1},V_{B2},V_{S2})=(-0.01325,-0.11,-0.11,0)$ V.

runs from 1 to 3, with $j=1$ representing the ground state. α, β, and γ are each functions of t_{LM} and t_{MR}. For ideal CTAP $\beta_2=0$ at all times. Notionally CTAP operates through maintaining the charge degree of freedom in the first-excited state, $|\Psi_2\rangle$, and adiabatically evolving $|\Psi_2\rangle$, such that the wave function is transferred from $|L\rangle$ at the start to $|R\rangle$ at the end through voltage tuning such that $\gamma_2=0$ at the start and $\alpha_2=0$ at the end. The first excited state $|\Psi_2\rangle$ is protected from $\Psi_1>$ and $\Psi_3>$ by energy gaps Δ_{12} and Δ_{23}, respectively. We will discuss later in this paper a method to project the multimillion atom Hamiltonian on to a 3×3 subspace, which can provide an accurate description of the full Hamiltonian for the relevant states. This model is one of the important contributions of this paper.

In Fig. 2, we show the molecular states of the triple donor system at the midpoint of the adiabatic transfer path for the CTAP protocol. E1 represents the ground state while E2 and E3 are the first and second excited states, respectively. CTAP transport takes effect through the state E2. In an ideal scenario, the middle donor between the barrier gates can be replaced by a chain containing an odd number of donors, and the same transfer protocol can still hold, without the need for any additional gates.[47]

In this work we will use the relative electron density in the center donor in the state E2 ($|\Psi_2\rangle$) as a metric of the efficacy of the CTAP transfer. The justification for this metric directly comes from earlier works.[8,16–18] Adiabatic transfer is realized through the wave function symmetries described earlier in this section and also shown in Fig. 2 for the midpoint of the adiabatic path. The vanishing center donor density in the state E2 ($|\Psi_2\rangle$) is a defining feature of this adiabatic transfer. Any marked build up of center donor density in E2 indicates a deviation of the wave-function symmetries required for CTAP, and is an indication that the transfer is becoming more nonadiabatic.

In Fig. 3, we performed a time-dependent analysis based on the effective 3×3 CTAP density matrix to show the relation between the donor densities in the adiabatic and nonadiabatic regimes. The time evolution of the densities was obtained from $d\rho/dt=-(i/\hbar)[H,\rho]$. We ignored effects of decoherence for this analysis as it is beyond the scope of this work, and was considered in Ref. 48 in the more general context of adiabatic information transport. To effect an electron transfer from donor L to donor R, CTAP relies on a counter-intuitive pulsing (CIP) of the barrier gates, in which B_2 is pulsed before B_1. On the other hand, the more conventional sequential transport from donor R to M and then to L is nonadiabatic in nature, and can be realized with an IP scheme, in which B_1 is pulsed before B_2. Figure 3 shows the Gaussian pulses [in Fig. 3(a)] and the evolution of the donor densities in time [in Figs. 3(b)–3(e)]. The IP sequence produces an oscillating donor density in the end donor R [Fig. 3(d)] and significant population in M [Fig. 3(e)] which oscillates in time. This pulse does not guarantee a robust final transfer to the end donor. The CIP scheme evolves the system adiabatically as the density in R [Fig. 3(b)] smoothly increases to 1 with vanishing density at M [Fig. 3(c)] at all times, making CTAP a robust transport method.

The build up of center donor density in E2 represents a deviation from ideal CTAP. Imperfections such as decoherence, straggle, and voltage noise can enhance this center density, taking the system into a more nonadiabatic transfer regime. The center donor density is thus a degree of measure of the nonideality of a CTAP transfer, as suggested also in Refs. 16–18.

III. METHOD

Since, in principle, CTAP is an adiabatic problem, we analyze it by solving the time independent Schrödinger equation at different bias points. We have employed the 10 band $sp^3d^5s^*$ tight-binding model with nearest-neighbor interactions. The model parameters were optimized by a genetic algorithm with appropriate constraints to reproduce the important features of the bulk band structure of the host.[40] The model parameters have been well established in the literature,[45,49] and calculations performed with these parameters have been verified against experimental measurements in a number of works.[41–43,46,50]

Each P donor was modeled by a Coulomb potential screened by the dielectric constant of Si. At the donor site, a cut-off potential U_0 was used, and its value optimized so that the ground-state binding energy of −45.6 meV was obtained for a donor in bulk Si. In this TB model, the valley-orbit interaction that lifts the sixfold degeneracy of the donor ground state is inherently included.[51]

The electrostatic gate potential was obtained from a commercial Poisson solver[52] for a single gate, and the potential for the three gates was treated as a superposition of the single gate solution. Although the voltages presented here will have some offsets from the realistic case due to this, the basic trends and analysis presented here are general, and this approach reduced the computational resources necessary to complete the calculations in a tractable time.

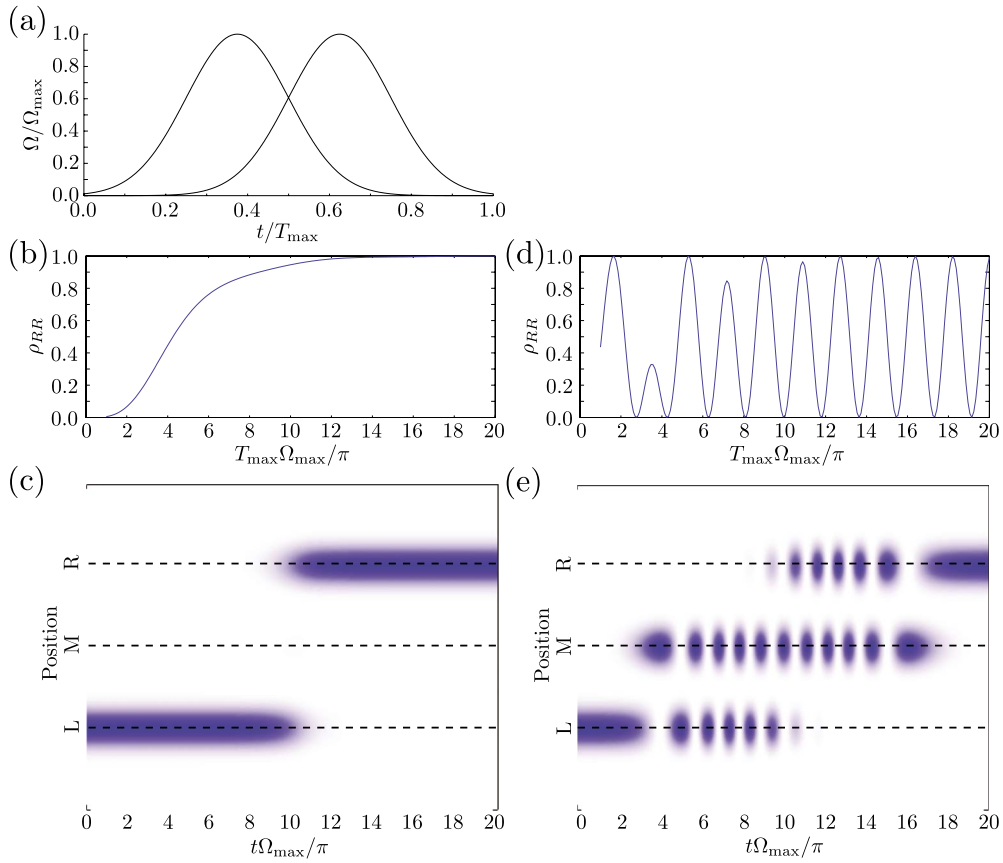

FIG. 3. (Color online) Population evolution through CTAP sequence. (a) For these calculations we use a Gaussian pulse sequence. For the intuitive direction, t_{LM} is the leading pulse, followed by t_{MR}. In the counter-intuitive direction, this order is reversed. (b) Final state population at donor $R(\rho_{RR})$ for increasing *total* time of the pulse sequence in the counterintuitive direction. Note the smooth, monotonic improvement in transfer fidelity with increasing time. (c) Population as a function of time through the CTAP protocol for total time $T_{\max}=20\pi/\Omega_{\max}$. Observe the smooth population transfer with negligible population at the central donor. (d) As (b) but for the intuitive pulse sequence. Note the oscillating population, with the final state population depending sensitively on the total time. (e) As (c) for the intuitive direction, again showing that the population exhibits nonadiabatic oscillations through the transfer protocol.

The net potential was then interpolated onto the atomistic grid for the tight- binding simulations. Closed boundary conditions with a model of dangling bond passivation was used to model the interfaces.[53] The full Hamiltonian of about 3.5 million atoms including the four gate potentials was solved by parallel Lanczos and block Lanczos algorithms to capture the relevant eigenvalues and wave functions. Typical computation time for a single time-step of the protocol over 6 states was 7 h on 40 processors.[54]

IV. RESULTS AND DISCUSSIONS

A. Binding energy of P_3^{2+} with straggle under zero gate bias

In a single P donor, the lowest manifold consists of 6 1s type orbital states, arising from the sixfold degenerate conduction band valleys of Si. Due to the valley-orbit interaction caused by central cell effects,[55] the six 1s states are split into an orbital singlet A_1, an orbital triplet T_2, and an orbital doublet E.[56] The A_1 state for a P donor is separated by 11.7 meV from the T_2 states. In a triple donor chain with donor separations much larger than the donor Bohr radii, the E1, E2, and E3 states arise from linear combinations of the A_1 states of each impurity. The 12 meV gap between the A_1 and the T_2 states of a single donor also gives rise to a significant energy gap between the lowest three states and the higher manifold of the P_3^{2+} molecule, which is a desirable condition for efficient CTAP transfer. Translation of this concept to quantum dots will be straightforward only if the valley splitting is large such that the lowest three states involved in CTAP are sufficiently isolated in energy from the valley split manifold.

In Fig. 4, we show the lowest energy states of the P_3^{2+} molecule at zero gate bias as a function of nonideal placement of the middle donor. ΔR represents the distance the middle donor is displaced toward the right donor relative to its ideal (equidistant) location. For example, in Fig. 4(a), $\Delta R=0.543$ nm means that the middle donor is displaced by one lattice constant a_0 (0543 nm) along the donor chain.

The states E2 and E3, which are degenerate at $\Delta R=0$, split due to asymmetric tunnel coupling to the left and right donors, as shown in Figs. 4(a)–4(c). The order of millielectron volt splitting for the range of donor separations considered here is comparable to the order of gate voltage modulation for electron transfer. Hence, donor straggle is likely to affect the adiabatic transfer. For large donor misplacements of $10a_0$ or more, there is the added problem that the higher

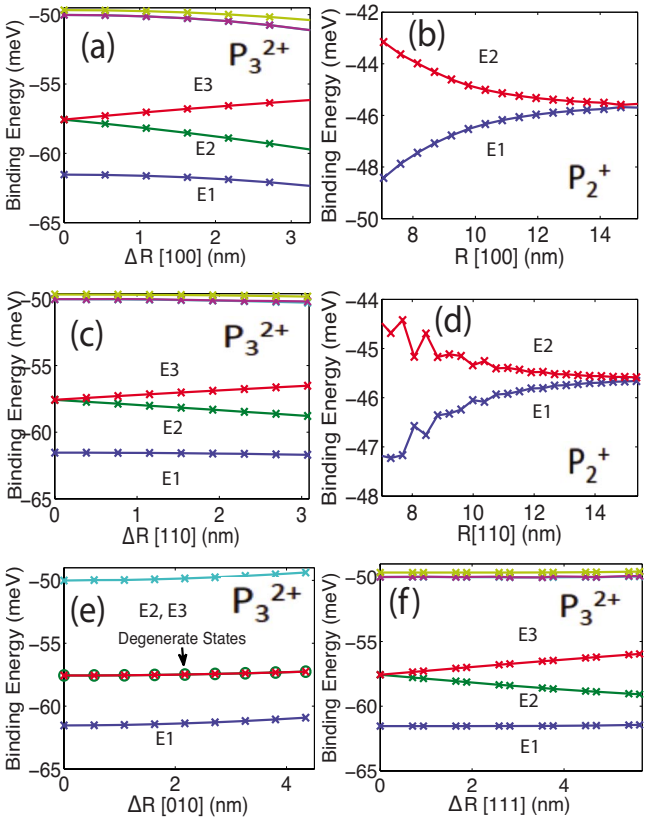

FIG. 4. (Color online) The lowest few states of the triple donor system at zero gate bias. The binding energy is expressed relative to the conduction band minima of Si. ΔR is the distance the middle donor is moved toward the right donor from the ideal (equidistant) case of 15.2 nm separation. The states for ΔR along (a) [100] (x), (c) [110] ($x=y$), (e) [010] (y), and (f) [111] ($x=y=z$). Plots (b) and (d) compare the lowest two (bonding and antibonding) states of a donor charge qubit (P_2^+) for donor separations along [100] (x) and [110] ($x=y$), respectively.

manifold of states move toward the second excited state E3, an undesirable condition for efficient transfer. This represents a potentially significant challenge to implement buried CTAP.

Figures 4(c) and 4(f) are for donor straggle along [110] and [111] directions, respectively, relative to the ideal chain in [100]. The striking feature is that the variations are almost smooth, compared to the oscillations in symmetric-antisymmetric energy states (Δ_{SAS}) for a charge qubit of P_2^+ molecule shown in Fig. 4(d) and also in Ref. 35. In the triple donor system, the oscillations in energy states with donor separations seem to be somewhat mitigated. This indicates that relatively smooth voltage corrections are possible.

Figure 4(e) shows the effect of straggle on the donor spectrum for a displacement perpendicular to the chain along [010] direction. In this case, the spectrum is less affected as the middle donor remains equidistant from the left and right donors. The states E2 and E3 remain degenerate throughout as expected.

B. Effect of straggle in donor position on the adiabatic path

To investigate the effect of straggle more exactly, we have chosen the midpoint of the adiabatic path shown in Fig. 2 for

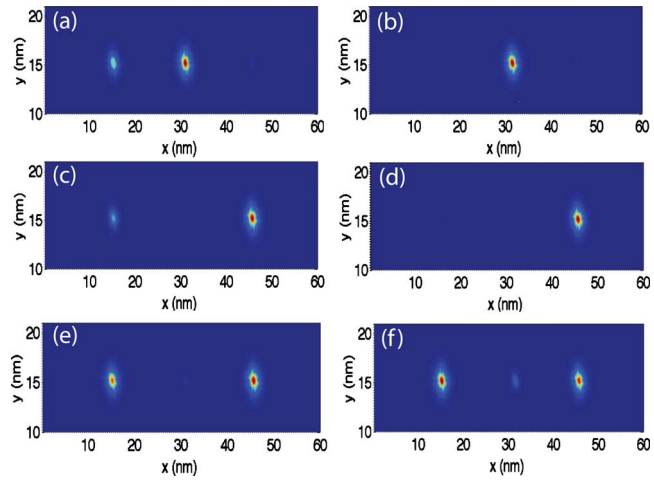

FIG. 5. (Color online) Plots of the first-excited state (E2) electron density for donor straggle of (a) $\Delta R=1a_0[100](x)$ ($a_0=0.543$ nm being the lattice constant of Si), (b) $\Delta R=2a_0[100](x)$, (c) $\Delta R=1a_0[010](y)$, (d) $\Delta R=2a_0[010](y)$, (e) $\Delta R=1a_0[100](x)$ with a corrective bias of $(-0.01325,-0.11,-0.11,-0.0084)$ V, and (f) $\Delta R=2a_0[100](x)$ with a corrective bias of $(-0.01325,-0.11,-0.11,-0.0170)$ V. Cases (e) and (f) are the same as cases (a) and (b), respectively, except a corrective voltage is applied to the S_2 gate.

the ideal case. Under the same gate bias, we have displaced the middle donor to neighboring lattice sites, and investigated the effect on the CTAP states. Since the basic parameters of interest in CTAP are the relative tunnel barriers between neighboring donors, we have concerned ourselves with relative displacements of the center donor from the left and the right donors only. In essence, absolute displacements of the outer donors have a similar effect as they produce the same asymmetric coupling investigated here. In particular, we compared the first-excited state E2 obtained in this manner with the ideal E2 shown in Fig. 2.

In Figs. 5(a) and 5(b), the middle donor is displaced by $1a_0$ and $2a_0$, respectively, toward the right donor (in [100] (x) direction). It is observed that the population becomes dominant at the center donor. If the donor is displaced perpendicular to the chain ([010] (y) direction) as in Figs. 5(c) and 5(d), the center donor density is still negligible. This suggests an intuition that straggle effects are maximum when donors are misplaced along the chain since the tunnel coupling is asymmetrically affected the most in such cases.

In Figs. 5(e) and 5(d), we have found voltages that can be applied to the S_2 gate to correct for the $1a_0$ and $2a_0$ straggle effects of Figs. 5(a) and 5(b), respectively, even in the presence of considerable perturbation from other neighboring gates. This means that external macroscopic voltages can be used to compensate for straggle effects due to single atom placement errors, which is a central point of this paper.

Similarly, in Fig. 6, we investigated the effect of donor displacement along [110] in Figs. 6(a) and 6(b), and along [111] in Figs. 6(c) and 6(d). These directions are expected to be more susceptible to rapid spatial oscillations of the host Bloch functions, as seen in two-donor charge qubits.[35] However, it is found that the center population is still somewhat negligible, which suggests that the effect of the

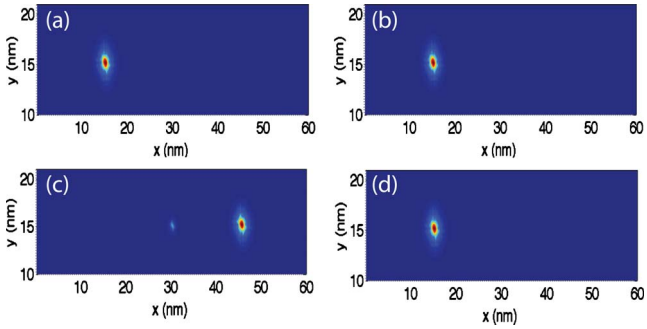

FIG. 6. (Color online) Plots of the first-excited state (E2) electron density for donor straggle of (a) $\Delta R=0.5a_0[110]$, (b) $\Delta R=1a_0[110]$, (c) $\Delta R=-0.25a_0[111]$, and (d) $\Delta R=0.75a_0[111]$.

crystal momentum states is not significant in this triple donor system.

C. Sensitivity of the protocol to gate voltage fluctuations

The transfer efficiency of the CTAP protocol in realistic systems may be susceptible to voltage noise. In particular, voltage fluctuations in the system can originate from charge traps or from small fluctuations in the gate pulses. Such variations are likely to affect both the tunnel barriers and the detuned energies of the donors, thereby introducing a finite population in the center donor.

In Fig. 7, we have again used the center donor population as a measure of the effectiveness of the transfer, and investigated the robustness of the adiabatic path to voltage fluctuations. For simplicity, we have modeled the voltage noise by perturbing V_{B1} by a percentage of its value at the midpoint of the adiabatic path.

Although Fig. 7 shows that such voltage offsets indeed introduce some population at the center, it is to be noted that center donor density remains considerably smaller for the more negative bias range. At −5% change in V_{B1}, the population at the center is still about 0.04 out of 1. However, the center donor density is very sensitive to the more positive

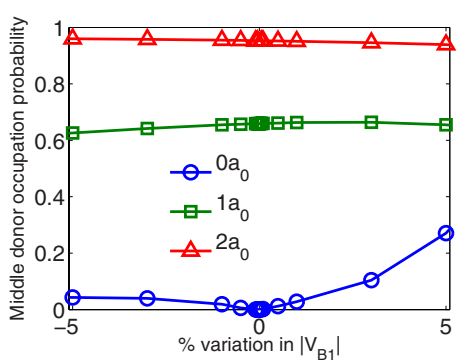

FIG. 7. (Color online) Sensitivity of the adiabatic pathway to fluctuations in the barrier gate voltage V_{B1}. The plot is for the mid point of the path with $(-0.01325,-0.11,-0.11,0)$ V for which the center donor population is $5.4e-4$ out of 1. The center donor density is plotted as a function of percentage variation in $|V_{B1}|$ for a range of −5 to +5 percent for the ideal case as well as straggle of 1 and 2 lattice constants along the chain.

bias range. The transfer efficiency is seriously hampered after +2−3 percent fluctuation in V_{B1}.

This asymmetry in sensitivity occurs due to the ordering of the CTAP states. As shown in Fig. 2, the state with the most central donor density is the second-excited state (E3) of the system. However, at zero gate bias, this state is the ground state of P_3^{2+} due to strong tunnel coupling between the donors. Negative barrier gate biases were required to rearrange the states to realize the adiabatic path. Hence, more positive gate biases causes this state to be either the first-excited state or ground state of the system, and thus breaks down the adiabatic path. Negative bias fluctuations, however, keep the ordering of the states intact, and have less effect on the path.

D. Effective 3×3 model developed from tight-binding

Problems such as CTAP and STIRAP are well described by small scale effective models, portrayed as a 3×3 matrix in the three-donor CTAP, for example. However, a complete and realistic description of the system has to include atomic scale effects from a method such as tight binding. In this section, we describe a procedure to translate a complex atomistic system into a simpler 3×3 matrix model that retains the relevant atomic scale information. Such a model is general beyond CTAP, and helps to bridge the gap between intensive atomistic theories and reduced order envelope function methods.

Although atomistic TB simulations capture the realistic features of a CTAP device and are useful to guide CTAP experiments of the future, a typical experiment will involve scanning over a large bias range with any number of possibilities for straggled donor positions. Thousands of large scale TB simulations to understand the device will be impractical and time consuming. For this purpose, we have developed an effective 3×3 model constructed from a few TB simulations of the system. In the perturbative regime, in which gate voltages cause small changes in the A_1 state of each impurity, this model can provide the same information as the actual TB solution of the full atomistic Hamiltonian. The advantage of this model is that a large number of voltages and straggled positions can be explored very rapidly, and correction procedures can be determined quickly. By imposing symmetry conditions and combining numerical parameterization and analytic solutions, we can even find sets of gate biases for various points of the adiabatic path, as we demonstrate below.

Assuming three different donor sites, and a wave function localized in each donor, we can use a 3×3 Hamiltonian describing the system in this three-state basis. This Hamiltonian H_{eff} is of the form,

$$H_{\text{eff}}=\begin{pmatrix} E_L & t_{LM} & t_{LR} \\ t_{LM^*} & E_M & t_{MR} \\ t_{LR^*} & t_{MR^*} & E_R \end{pmatrix}, \tag{3}$$

where E_i is the on-site energy of the ith impurity, and t_{ij} is the tunneling matrix element from impurity i to impurity j. If

the on-site energies of the donors are aligned closely, the tunneling elements t_{LM} and t_{MR} can be switched alternately from on to off adiabatically to effect the electron transfer.[39]

The idea is to make this model more realistic by calculating the matrix elements from atomistic TB simulations. The TB Hamiltonian for a single donor under zero gate bias is given by, $H_i = H_0 + V_i(R_i)$, where H_0 is the crystal Hamiltonian, and V_i is the core corrected Coulomb potential of impurity $i = L, M, R$ located at $R_i = R_L, R_M, R_R$. If we solve for H_i for each of the three donors separately, we can obtain a set of donor states $\{\psi_{ji}\}$, where j is the state index, and i is the impurity index. In this case, we restrict our attention to the donor ground state only. So, $j=1$, and $i=L,M,R$, and the basis set $\phi = \{\psi_{1L}, \psi_{1M}, \psi_{1R}\}$. The full TB Hamiltonian of the CTAP device is,

$$H_T = H_0 + V_L(R_L) + V_M(R_M) + V_R(R_R) + V_G(V_{S1}, V_{B1}, V_{B2}, V_{S2}). \quad (4)$$

The matrix elements of H_{eff} is then given by, $[H_{\text{eff}}]_{lk} = \langle \psi_{1l} | H_T | \psi_{1k} \rangle$. Whereas the full solution of H_T is time intensive, requiring many matrix vector multiplications in Lanczos, it is fairly fast to evaluate each matrix element of the 3×3 model as it involves one matrix vector multiplication between the TB Hamiltonian and a vector, and one inner product between two vectors. Since the basis set Φ is nonorthogonal, the 3×3 problem to be solved is of the form, $H_{\text{eff}}\phi = ES\phi$, where S is the overlap matrix with elements $S_{lk} = \langle \psi_{1l} | \psi_{1k} \rangle$. The eigen solution of the H_{eff} gives the molecular states of the CTAP device in the basis of the A_1 states of the three donors. It is to be noted that by simply including the donor excited states in the basis (for $j > 1$), the model can be made more comprehensive and applicable to other donor related problems as well. It is also fairly easy to extend this method to any number of donors.

Our approach at this point is to find the functional dependencies of the matrix elements on the four gate biases V_G, and atomic straggle as captured in the donor potential $V_i(R_i)$. In our case, we were able to perform linear fits of all the elements to the gate biases, with the function,

$$[H_{\text{eff}}]_{lk} = a_1 V_{S1} + a_2 V_{B1} + a_3 V_{B2} + a_4 V_{S2} + a_5, \quad (5)$$

where the coefficients a_i are constants determined from the fit. Figure 8(a) shows some diagonal elements as a function of V_{B1} while Fig. 8(b) shows the same for the off-diagonal elements.

Once this parameterized 3×3 is obtained, we verify that the model is capable of deducing the voltages for the adiabatic path. To obtain the midpoint of the path, we impose the conditions $t_{LM} = t_{MR}$, $E_L = E_M = E_R$, and $V_{S1} = V_{S2} = 0$, and obtain the voltages, $V_{B1} = -0.1128$ V and $V_{B2} = -0.0903$ V from the matrix elements of H_{eff}. These voltages are offset minutely from our brute force simulations by 0.01325 V, 0.0028 V, and 0.0197 V for V_{S1}, V_{B1}, and V_{B2}, respectively. Performing the actual TB simulations with these voltages, we are able to obtain the midpoint of the adiabatic path, as shown by the wave-function symmetry in Fig. 8(c). In fact, we obtained an improvement over our previous voltages, of using only two gates instead of three. Therefore, the model is helpful for rapid evaluation of straggle effects.

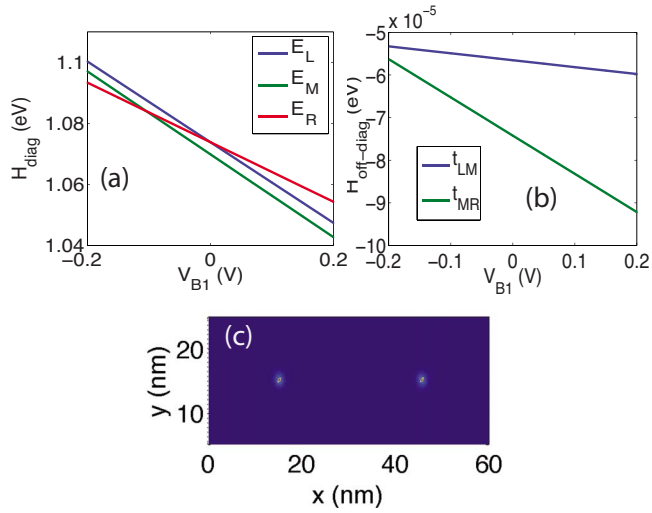

FIG. 8. (Color online) (a) Diagonal elements (E_L, E_M, E_R) of the 3×3 matrix as a function of V_{B1}. The other gates are set to zero. The donor M is equidistant from L and R. (b) The off-diagonal elements (t_{LM} and t_{MR}) with V_{B1}. (c) The state E2 obtained in TB from the bias set $(0, -0.1128, -0.0903, 0)$ V.

V. CONCLUSION

In this work, we investigated the effect of imperfections on coherent electron transport by adiabatic passage in a test triple donor system. Donor misplacements can severely hamper the adiabatic transfer path if the misplacements are along the chain but can be retuned in theory, which is a central conclusion of this paper. We also performed a study of the sensitivity of the path to gate voltage fluctuations showing non-negligible sensitivity. We developed a quick and easy way to bridge between large scale tight-binding simulations and possible CTAP experiments. The effective 3×3 model that we developed from TB simulations for this purpose also unites the atomic scale precision of TB with intuitive simplicity of a toy model. The model in conjunction with tight binding can help guide experiments even in the presence of imperfections such as donor straggle and gate voltage fluctuations. Furthermore, the model provides a general translation of intensive atomic scale calculations to simplified models used to describe problems in many solid-state and quantum-optics applications.

ACKNOWLEDGMENTS

This work was supported by the Laboratory Directed Research and Development program at Sandia National Laboratories and by the National Security Agency Laboratory for Physical Sciences under Contract No. EAO-09-0000049393. Sandia is a multiprogram laboratory operated by Sandia Corporation, a Lockheed Martin Co., for the United States Department of Energy under Contract No. DE-AC04-94AL85000. Part of the development of NEMO-3D was initially performed at JPL, Caltech under a contract with

NASA. NCN/nanohub.org computational resources were used. This work was supported by the Australian Research Council, NSA, and ARO (Contract No. W911NF-08-1-0527). A.D.G. and L.C.L.H. acknowledge the Australian Research Council for financial support (Projects No. DP0880466 and No. DP0770715, respectively). R.R. also acknowledges discussions with T. Gurrieri and R. Young of SNL.

*rrahman@sandia.gov
†rmuller@sandia.gov

[1] B. E. Kane, Nature (London) **393**, 133 (1998).
[2] R. Vrijen, Eli Yablonovitch, K. Wang, H. W. Jiang, A. Balandin, V. Roychowdhury, T. Mor, and D. Divincenzo, Phys. Rev. A **62**, 012306 (2000).
[3] C. D. Hill, L. C. L. Hollenberg, A. G. Fowler, C. J. Wellard, A. D. Greentree, and H.-S. Goan, Phys. Rev. B **72**, 045350 (2005).
[4] D. Loss and D. P. Vincenzo, Phys. Rev. A **57**, 120 (1998).
[5] S. Goswami, K. A. Slinker, M. Friesen, L. M. McGuire, J. L. Truitt, C. Tahan, L. J. Klein, J. O. Chu, P. M. Mooney, D. W. Van Der Weide, R. Joynt, S. N. Coppersmith, and M. A. Eriksson, Nat. Phys. **3**, 41 (2007).
[6] L. C. L. Hollenberg, A. S. Dzurak, C. Wellard, A. R. Hamilton, D. J. Reilly, G. J. Milburn, and R. G. Clark, Phys. Rev. B **69**, 113301 (2004).
[7] L. C. L. Hollenberg, A. D. Greentree, A. G. Fowler, and C. J. Wellard, Phys. Rev. B **74**, 045311 (2006).
[8] A. D. Greentree, Jared H. Cole, A. R. Hamilton, and L. C. L. Hollenberg, Phys. Rev. B **70**, 235317 (2004).
[9] V. Vitanov, T. Halfmann, B. Shore, and K. Bergmann, Annu. Rev. Phys. Chem. **52**, 763 (2001).
[10] S. Longhi, Phys. Rev. E **73**, 026607 (2006).
[11] S. Longhi, J. Phys. B **40**, F189 (2007).
[12] S. Longhi, G. Della Valle, M. Ornigotti, and P. Laporta, Phys. Rev. B **76**, 201101(R) (2007).
[13] K. Eckert, M. Lewenstein, R. Corbalan, G. Birkl, W. Ertmer, and J. Mompart, Phys. Rev. A **70**, 023606 (2004).
[14] K. Eckert, J. Mompart, R. Corbalan, M. Lewenstein, and G. Birkl, Opt. Commun. **264**, 264 (2006).
[15] E. M. Graefe, H. J. Korsch, and D. Whitthaut, Phys. Rev. A **73**, 013617 (2006).
[16] M. Rab, J. H. Cole, N. G. Parker, A. D. Greentree, L. C. L. Hollenberg, and A. M. Martin, Phys. Rev. A **77**, 061602(R) (2008).
[17] J. H. Cole, A. D. Greentree, L. C. L. Hollenberg, and S. Das Sarma, Phys. Rev. B **77**, 235418 (2008).
[18] T. Opatrný and K. K. Das, Phys. Rev. A **79**, 012113 (2009).
[19] L. M. Jong, A. D. Greentree, V. I. Conrad, L. C. L. Hollenberg, and D. Jamieson, Nanotechnology **20**, 405402 (2009).
[20] L. M. Jong and A. D. Greentree, Phys. Rev. B **81**, 035311 (2010).
[21] D. Schröer, A. D. Greentree, L. Gadreau, K. Eberl, L. C. L. Hollenberg, J. P. Kotthaus, and S. Ludwig, Phys. Rev. B **76**, 075306 (2007).
[22] K. Grove-Rasmussen, H. I. Jrgensen, T. Hayashi, P. E. Lindelof, and T. Fujisawa, Nano Lett. **8**, 1055 (2008).
[23] L. Gaudreau, A. S. Sachrajda, S. Studenikin, A. Kam, F. Delgado, Y. P. Shim, M. Korkusinski, and P. Hawrylak, Phys. Rev. B **80**, 075415 (2009).
[24] S. Amaha, T. Hatano, T. Kubo, S. Teraoka, Y. Tokura, S. Tarucha, and D. G. Austing, Appl. Phys. Lett. **94**, 092103 (2009).
[25] M. Pierre, R. Wacquez, B. Roche, X. Jehl, M. Sanquer, M. Vinet, E. Prati, M. Belli, and M. Fanciulli, Appl. Phys. Lett. **95**, 242107 (2009).
[26] A. J. Skinner, M. E. Davenport, and B. E. Kane, Phys. Rev. Lett. **90**, 087901 (2003).
[27] S. R. Schofield, N. J. Curson, M. Y. Simmons, F. J. Rue, T. Hallam, L. Oberbeck, and R. G. Clark, Phys. Rev. Lett. **91**, 136104 (2003).
[28] F. J. Ruess, B. Weber, K. E. J. Goh, O. Klochan, A. R. Hamilton, and M. Y. Simmons, Phys. Rev. B **76**, 085403 (2007).
[29] F. J. Ruess, W. Pok, K. E. J. Goh, A. R. Hamilton, and M. Y. Simmons, Phys. Rev. B **75**, 121303(R) (2007).
[30] Simmons group unpublished work (2009–2010).
[31] M. Fuechsle, S. Mahapatra, F. A. Zwanenburg, M. Friesen, M. A. Eriksson, and M. Y. Simmons, Nat. Nanotechnol. **5**, 502, (2010).
[32] D. N. Jamieson, C. Yang, T. Hopf, S. M. Hearne, C. I. Pakes, S. Prawer, M. Mitic, E. Gauja, S. E. Andresen, F. E. Hudson, A. S. Dzurak, and R. G. Clark, Appl. Phys. Lett. **86**, 202101 (2005).
[33] J. A. Van Donkelaar, A. D Greentree, A. D. C. Alves, L. M. Jong, L. C. L. Hollenberg, and D. N. Jamieson, New J. Phys. **12**, 065016 (2010).
[34] B. Koiller, X. Hu, and S. Das Sarma, Phys. Rev. Lett. **88**, 027903 (2001).
[35] X. Hu, Belita Koiller, and S. Das Sarma, Phys. Rev. B **71**, 235332 (2005).
[36] J. H. Cole, S. G. Schirmer, A. D. Greentree, C. J. Wellard, D. K. L. Oi, and L. C. L. Hollenberg, Phys. Rev. A **71**, 062312 (2005).
[37] J. H. Cole, A. D. Greentree, D. K. L. Oi, S. G. Schirmer, C. J. Wellard, and L. C. L. Hollenberg, Phys. Rev. A **73**, 062333 (2006).
[38] M. J. Testolin, C. D. Hill, C. J. Wellard, and L. C. L. Hollenberg, Phys. Rev. A **76**, 012302 (2007).
[39] R. Rahman, S. H. Park, J. H. Cole, A. D. Greentree, R. P. Muller, G. Klimeck, and L. C. L. Hollenberg, Phys. Rev. B **80**, 035302 (2009).
[40] J. C. Slater and G. F. Koster, Phys. Rev. **94**, 1498 (1954).
[41] R. Rahman, C. J. Wellard, F. R. Bradbury, M. Prada, J. H. Cole, G. Klimeck, and L. C. L. Hollenberg, Phys. Rev. Lett. **99**, 036403 (2007).
[42] S. H. Park, R. Rahman, G. Klimeck, and L. C. L. Hollenberg, Phys. Rev. Lett. **103**, 106802 (2009).
[43] G. P. Lansbergen, R. Rahman, C. J. Wellard, I. Woo, J. Caro, N. Collaert, S. Biesemans, G. Klimeck, L. C. L. Hollenberg, and S. Rogge, Nat. Phys. **4**, 656 (2008).
[44] R. Rahman, G. P. Lansbergen, S. H. Park, J. Verduijn, G. Klimeck, S. Rogge, and L. C. L. Hollenberg, Phys. Rev. B **80**, 165314 (2009).
[45] G. Klimeck, F. Oyafuso, T. B. Boykin, R. C. Bowen, and P. V.

Allmen, Comput. Model. Eng. Sci. **3**, 601 (2002).

[46] G. Klimeck, S. Ahmed, N. Kharche, M. Korkusinski, M. Usman, M. Prada, and T. Boykin, IEEE Trans. Electron Devices **54**, 2079 (2007).

[47] A. D. Greentree, J. H. Cole, A. R. Hamilton, and L. C. L. Hollenberg, *Micro-and Nanotechnology: Materials, Processes, Packaging and Systems II*, Proceedings of SPIE Vol. 5650 (University of NSW, Sydney, 2005), p. 72.

[48] I. Kamleitner, J. Cresser, and J. Twamley, Phys. Rev. A **77**, 032331 (2008).

[49] T. B. Boykin, G. Klimeck, and F. Oyafuso, Phys. Rev. B **69**, 115201 (2004).

[50] N. Kharche, Marta Prada, T. B. Boykin, and G. Klimeck, Appl. Phys. Lett. **90**, 092109 (2007).

[51] S. Ahmed, N. Kharche, R. Rahman, M. Usman, S. Lee, H. Ryu, H. Bae, S. Clark, B. Haley, M. Naumov, F. Saied, M. Korkusinski, R. Kennel, M. McLennan, T. B. Boykin, and G. Klimeck in *Springer Enclycopedia for Complexity*, edited by R. A. Meyers, (Springer, Berlin, 2009), p. 681.

[52] The electrostatic gate modeling was done using ISE TCAD in CQCT, Melbourne, Australia.

[53] S. Lee, F. Oyafuso, P. von Allmen, and G. Klimeck, Phys. Rev. B **69**, 045316 (2004).

[54] NanoHUB.org computational resource of a 256-node 3.3GHz Pentium Irvindale PC cluster was used in this work. The tight-binding calculations were done using the Nano-Electronic Modeling Tool (NEMO-3D).

[55] A. K. Ramdas and S. Rodriguez, Rep. Prog. Phys. **44**, 1297 (1981).

[56] W. Kohn and J. M. Luttinger, Phys. Rev. **98**, 915 (1955).